Technical Notes

Propellant Triggered Gas Discharges in Pulsed Plasma Engines

M. E. Levy*
Vitro Laboratories, West Orange, N. J.
AND
A. J. Schwalb†
Walter Kidde and Company Inc., Belleville, N. J.

PLASMA accelerators operated in this[1] and other laboratories utilize gas propellant introduced by a pulsed valve mechanism through small orifices in one of the electrodes. The injected gas propellant triggers the electrical discharge in the accelerator and is subsequently accelerated by a pinching process. Experimental evidence[2] shows that the plasma accelerator performance depends critically upon the propellant gas density in the interelectrode space just prior to the electrical discharge. If this density distribution is known, the total propellant mass in the interelectrode space can be calculated, and an appropriate magnetohydrodynamic model such as "Snowplow"[2] or "Slug"[3] can then be chosen to calculate the performance parameters for the accelerator.

The object of this study is to gain detailed knowledge of the events occurring within the accelerator between the time the injection valve is pulsed and the time appreciable current starts flowing in the discharge. This involves the development of analytical expressions for the space-time distribution of neutral gas-propellant density in the interelectrode space and the establishment of the sequence of events leading to electrical breakdown.

The understanding of the electrical breakdown process is complicated by the fact that electrical breakdown conditions cannot be well defined in a flow environment where density gradients exist. Breakdown conditions in static gases can be predicted by the Paschen relationship.[4,5] In flowing gases, only limited experimental results are available.[6,7] Part of the work reported here is devoted to an examination of the electrical breakdown conditions in a flow field characterized by density gradients.

In these experiments the accelerator electrodes are replaced by two flat, circular, parallel plates in a linear pinch configuration. Propellant is injected from the propellant reservoir tank by a pulsed valve, through a duct leading to a single orifice in the center of one of the electrodes.

An analytical model is introduced that reflects the physical aspects of the neutral gas injection mechanism (Fig. 1). The valve is represented as a diaphragm separating the propellant at uniform pressure and density from a vacuum in a constant area duct. This duct, which simulates the propellant supply passages, discharges into the interelectrode space that is evacuated. Propellant fluid injection is accomplished by virtue of the pressure differential across this diaphragm. The diaphragm is assumed to burst instantaneously, simulating a very fast acting valve.

Thus, upon instantaneous removal of the diaphragm ($t = 0$), the propellant gas flows down the constant area injection port

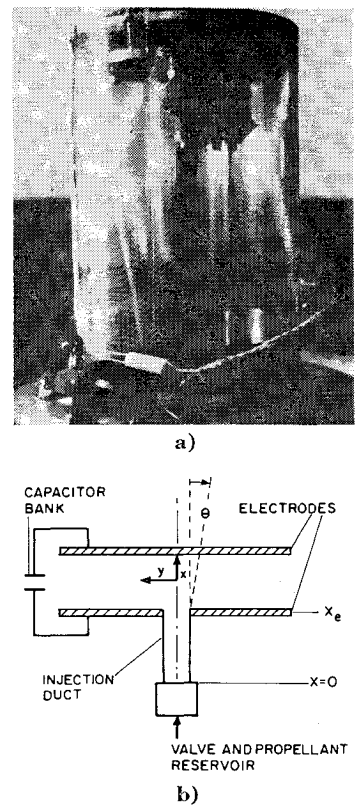

Fig. 1 Photograph and schematic diagram of apparatus.

and is described by the following inviscid, isentropic, continuum one-dimensional unsteady flow relationships for the nondimensionalized density, velocity, and mass flow ratio distributions:

$$\rho/\rho_i = [2/(\gamma + 1) - (\gamma - 1)/(\gamma + 1)x/(a_i t)]^{2/(\gamma-1)} \quad (1)$$

$$u/a_i = 2/(\gamma + 1)[1 + x/(a_i t)] \quad (2)$$

$$\rho u/\rho a_i = (\rho/\rho_i)(u/a_i) \quad (3)$$

where γ and a_i are the specific-heat ratio and the initial speed of sound in the fluid, respectively. The resulting nondimensionalized density distribution in the duct is given in Fig. 2.

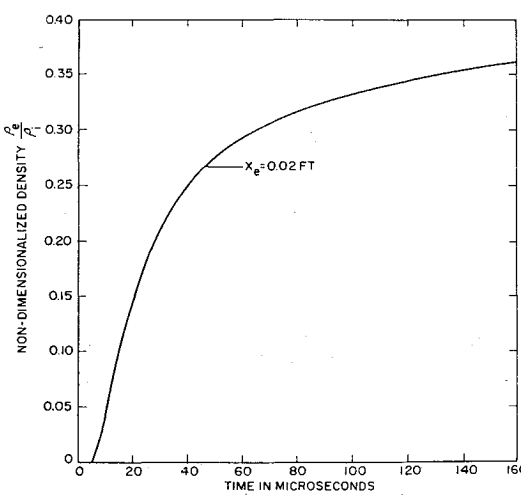

Fig. 2 Density distribution for unsteady flow in a constant area tube.

Presented as Preprint 64-707 at the AIAA Fourth Electric Propulsion Conference, Philadelphia, Pa., August 31–September 2, 1964; revision received May 10, 1965. This work was performed at Republic Aviation Corp., Farmingdale, N. Y. The authors wish to thank W. McIllroy of Republic Aviation for his helpful suggestions.

* Physicist, Physics and Space Sciences Department.
† Consultant Aero-Space Division.

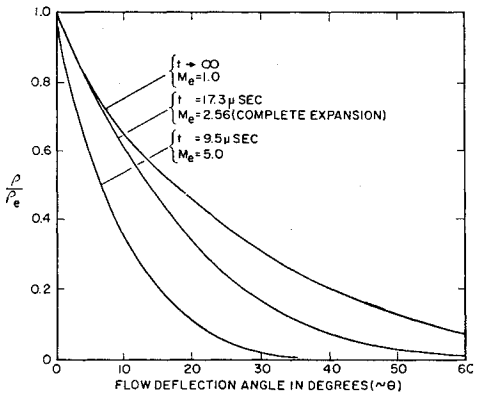

Fig. 3 Density distribution through Prandtl-Meyer expansion fan as a function of flow-deflection angle.

Analysis of the relations (1–3) for the application cited here, namely an injection port length of 0.02 ft, results in the following two important flow features: 1) continuum flow is established very rapidly in less than 10 μsec in the propellant injection duct (it should be noted that this time interval is short compared to the process leading to electrical breakdown, and thus rarefied gas effects are negligible) and 2) steady-state conditions in the propellant injection duct are attained in 40 μsec. Therefore, the fluid expansion occurring at the end of the duct into the interelectrode space is assumed to be a two-dimensional quasi-steady Prandtl-Meyer flow, where the initial conditions are the known time varying conditions at the duct exit station given by Eqs. (1–3).

The equations describing the two-dimensional Prandtl-Meyer expansion are 1) the integrated expression obtained from the approximation for the change of speed across a weak shock $du/u = -d\theta/(M^2 - 1)^{1/2}$, 2) the geometrical consideration $\theta = \mu \pm \beta$, and 3) the steady flow isentropic equations where θ, μ, and β are the flow-deflection angle, the Mach angle ($\mu \equiv \sin^{-1}1/M$), and the characteristic direction angle ($dy/dx \equiv \tan\beta$), respectively.

Using the quasi-steady model, the density distributions in the flow field were determined as a function of flow deflection angle θ measured from the x axis for times approaching breakdown conditions (Fig. 3). This density distribution obtained in the interelectrode space indicates that the mass is essentially concentrated in a collimated beam, since lateral spreading is incomplete.

The experimental apparatus is shown schematically in Fig. 1. The basic equipment consists of a solenoid operated valve requiring approximately 2 Joules per activation, and a set of circular flat aluminum electrodes in a linear pinch configuration. The lower electrode has an orifice in the center (0.073 in., $\frac{1}{2}$-in. long) through which gas is pulsed into the interelectrode spacing by the valve.

The valve is operated by a timing circuit, and the rise and open time characteristics of the plunger movement are completely determined by the activating electrical pulse. A minimum activation gives an open time of 6μsec. The valve was operated with an open time of 10 μsec throughout. The random delay of plunger lift time for identical activation pulses was ±20 μsec. Nitrogen gas was used. There exists a linear relationship between the gas pressure behind the valve before pulsing P_i and the mass injected.

The electrodes are connected across a capacitor bank, and have been used at a spacing of $\frac{1}{2}$ in. The ringing frequency of the system is 52 kc. Part of the system, including valve and electrodes, was fitted under a bell jar vacuum chamber (Fig. 1).

Time integrated and streak photography were used to photograph the luminous discharge event. The energy of the discharges was obtained from a 10 μfarad capacitor charged to different voltages in the range between 500 and 2000 v. The resulting luminosity in the N_2 gas during a discharge was assumed to be qualitatively related to the density distribution of the propellant in the interelectrode region. Typical data are shown in Figs. 4 and 5.

The delay time between valve opening (plunger lift off) and the occurrence of the discharge was studied as a function of the initial pressure P_i behind the injection valve and the initial voltage across the electrodes. The discharge is defined to occur at the time when high currents (of the order of 200 amp) start flowing between the electrodes and was experimentally detected using both Rogowski coils and voltage dividers. The plunger lift off was monitored through a hole in the valve body. A light beam crossing this hole exposed a phototube when the plunger would start opening, thus providing reliable detection of plunger motion.

A fast response sensitive density probe was used to measure time of arrival of the injected gas front into the interelectrode space. These measurements, conducted for two different pressures, are tabulated in Table 1 in terms of the resulting velocities. The density probe operated on the principle of the Penning discharge and is fully described in the literature.[8]

The density distribution of the propellant at the time of electrical discharge for several mass flow values and electrical potentials is deduced from the time integrated and time resolved photographs (Figs. 4 and 5) and is in qualitative agreement with the theoretical density distribution given as a function of the cone ray half-angle shown in Fig. 3. In each case the luminosity from ion-electron recombination and relaxation of excited states is observed. This luminosity is proportional to propellant density and is established at a rate such that the propellant distribution does not change appreciably during the observation, therefore affording an instantaneous visualization of the flow field. It appears that the propellant injection jet travels almost undispersed, with the highest density concentrated in a small cone with apex at the injection orifice and the base on the opposite electrode. The point of initial electrical breakdown clearly coincides with the high-density regions in the neutral gas. It would seem therefore, that propellant density is instrumental in determining the spatial characteristics of the initial breakdown.

It is apparent that for this mode of propellant injection, when the discharge occurs, the gas may be considered in the form of a "slug." The gas column being ejected from the orifice remains relatively undispersed during its travel to the opposite electrode. Upon collision with the opposite electrode, the gas particles of the ejected propellant column become randomized and are eventually pumped out of the interelectrode space by the ambient vacuum. An order-of-magnitude calculation of the pumping rate indicates that a mass of gas flowing at the mass flow rates used here ($\Delta m/\Delta t = 2 \times 10^{-4}$ lb/sec), will be pumped out of the interelectrode space fast enough so that the bulk of the mass available during

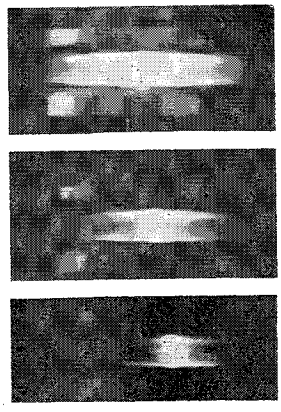

a) 1500-v discharge

b) 1000-v discharge

c) 500-v discharge

Fig. 4 Time integrated pictures of discharges (P_i = 200 mm of Hg, d = $\frac{1}{2}$ in.) taken with no. 1 neutral density filter.

Table 1 Gas front velocities

P_i, mm of Hg	Time of flight measured From d_1 = 1.4 in. To d_2 = 2.4 in.	From d_1 = 2.4 in. To d_2 = 3.4 in.
50	2064 fps ±50%	286 fps ±20%
100	2356 fps ±50%	452 fps ±20%

the acceleration process will be the part flowing in the propellant column at the instant of the high-current discharge.

The value of the velocity of the propellant gas as measured along with orifice axis should not depend on the initial pressure P_i of the propellant reservoir, and such is the case within experimental error. The value obtained near the orifice, in the 1.4 to 2.4 in. interval, is seen to be (Table 1) of the order of 2140 fps. This value falls between the theoretical mass average velocity 1615 fps given by $\{(2/\gamma)a_i\}$ and the theoretical velocity 2710 fps predicted by one-dimensional unsteady wave propagation theory.

The velocities measured further away from the orifice axis, within the 2.4 to 3.4 in. interval are much lower than theoretically predicted. The theory, however, predicts that a given density front or wavelet should travel at constant velocity and that the leading wavelets will have a higher velocity than those that follow. The discrepancy, though, can be explained in terms of the characteristics of the density gage used to obtain these velocity measurements.

The discharge gage is a threshold instrument of certain sensitivity and, as such, it indicates the time of arrival at a point of a transient density front whose density equals or exceeds the minimum density detectable. Close to the orifice, the density fronts or wavelets are close together, thus creating a high enough integrated density over a volume to be immediately detected by the density gage. At longer distances, however, the initial wavelets are separated from the ones that follow, since they travel at different velocities, and thus the integrated density over a small volume decreases. In this manner, the density wave detected at the furthest station is not the same one detected at the nearer point (because that one is below detection threshold) but a later one. The apparent velocities, as calculated from the time of arrival data at the points 1.4, 2.4, and 3.4 in. away from the orifice and along its axis should, as indeed they do, become progressively smaller than the ones predicted by one-dimensional unsteady wave propagation theory. The velocity measured in the 1.4 to 2.4 in. interval is, as expected, lower than the theoretically predicted velocity, about 2140 fps as compared to the expected 2710 fps. The agreement between theory and experiment is enhanced when one takes into consideration the density gage effect.

The results of the study of the time delay between initial penetration of the gas propellant into the interelectrode space and electrical breakdown as a function of reservoir pressure P_i and interelectrode potential are given in Fig. 6.

The solenoid pulsed valve used for these experiments has a rise time of 1.7 μsec from the fully closed position to the fully opened position. The applied pulse of 10 μsec duration provides a period between rise and fall of steady-state flow

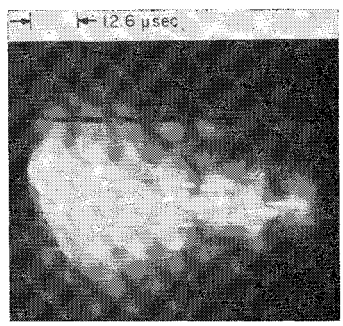

Fig. 5 Streak photograph of discharge in linear pinch geometry (2500 v, P_i = 200 mm of Hg, lower electro positive, upper electrode ground).

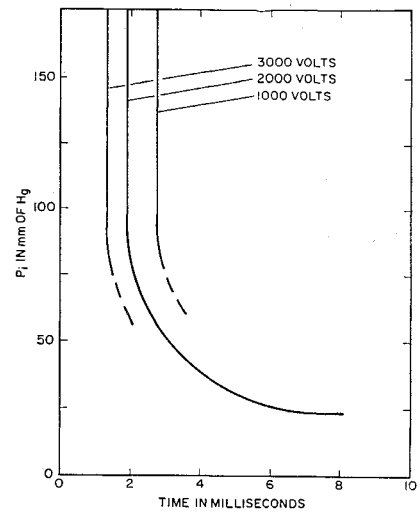

Fig. 6 Discharge delay vs propellant reservoir pressure P_i.

through the orifice of about 6.6 μsec. It has already been indicated that continuum, steady-state flow is established in times short compared to the valve open time.

The time delay between initial gas flow out of the orifice and the initiation of the discharge as defined in the foregoing depends on the potential across the charged plates and the mass flow rate (controlled through P_i). The breakdown delay is seen to decrease with increasing potential across the discharge plates. Such a result is fully expected.

The behavior of the delay time with respect to P_i is more complex. For low-reservoir pressures, one obtains progressively larger delays up to a cut-off point, where discharge cannot be initiated at all because of insufficient mass density build-up in the interelectrode space. In such a case, the breakdown conditions for the particular voltage are never realized. For high-reservoir pressures (high mass flow rates), breakdown conditions are reached faster, and the delay becomes progressively shorter. At initial pressures above a certain pressure (in the present case approximately 100 mm Hg) though, the time delay becomes asymptotic. Any further increase in mass flow rate does not result in a decrease in the delay time. This asymptotic dependence could not be attributed to choking in the injection channel, since it is found experimentally that no choking takes place up to initial pressures of 250 mm of Hg. This minimum delay, therefore, cannot be explained in terms of the presence of insufficient propellant mass to create breakdown conditions and therefore must be attributed to the electrical breakdown mechanism that is part of the chain of events leading to high-current flow.

The sequence of events that lead to electrical breakdown can be considered in the following manner. The valve opens, and the density between the electrodes begins to rise. At some point the (ρd) parameter (density times electrode gap) attains a breakdown value. A formative period for the discharge ensues, and then high current starts flowing (of the order of 200 amp threshold) indicating that breakdown has occurred. By specifying the voltage and the initial propellant pressure, one can control the time at which the firing of the accelerator would occur, within limits, which are indicated by the minimum breakdown pressure and voltage curves (Fig. 6), and the minimum time delay dictated by the valve characteristics.

An estimate of the current formative time delay in a flow-field characterized by density gradients can be obtained from the asymptotic value of the total breakdown delay time at initial pressures above 100 mm of Hg (Fig. 6). For this range of P_i, the total delay can be attributed mostly to the formative time required by the current. This time is of the order of 2 μsec and depends on discharge voltage.

The results presented here agree qualitatively with results obtained by Denichev and Matyukhin[9] with a coaxial accel-

erator operated by gas injection and used for the introduction of plasmoids into magnetic traps.

References

[1] Pearson, J., Cavalconte, C., Guman, W., and Granet, I., "Design, fabrication and test of a pulsed plasma engine for space applications," *Proceedings, Engineering Aspects of MHD*, edited by C. Manual and N. W. Mather (Columbia University Press, New York, 1962), pp. 81–96.

[2] McIlroy, W. and Siegel, B., "Analysis of factors influencing plasma engine performance," American Society of Mechanical Engineers Paper 63-AHGT-62 (1963).

[3] Mostov, P., Neuringer, J., and Rigney, D., "Electromagnetic acceleration of a plasma slug," Phys. Fluids **4**, 1097–1104 (1961).

[4] Loeb, L. B., *Fundamental Processes of Electrical Discharges in Gases* (John Wiley & Sons, Inc., New York, 1959).

[5] Brown, S. C., *Basic Data of Plasma Physics* (John Wiley & Sons, Inc., New York, 1959).

[6] Maier, F., "Glow discharge in high velocity gas streams," Z. Physik **93**, 65–85 (1934).

[7] Fucks, W., "Dependence of breakdown on dark current and frequency," Appl Sci. Res. **B5**, 109–23 (1955).

[8] Levy, M. E., "Discharge gauge for transient density measurements," Rev. Sci. Instr. **35**, 1232–1233 (September 1964).

[9] Denichev, V. F. and Matyukhin, V. D., Akad. Nauk SSSR, Doklady, **150**, 279–282 (May 1963).

Cross-Flow Effects in the Plane-Wall Jet

L. G. NAPOLITANO* AND F. MANZO†

Aerodynamics Institute, University of Naples, Italy

THE similar plane laminar wall jet was first considered in Ref. 1. A more general treatment was given by Glauert[2] who dealt, in an unified manner, with both the plane and axysymmetric cases and gave closed-form solutions. The object of this note is to discuss two instances of the laminar wall jet with cross flow. Specifically, we shall consider the similar flow fields due to 1) a two-dimensional jet impinging diagonally (i.e., nonorthogonally) on an infinite plane, and 2) a jet flowing over both sides of a semi-infinite plate that moves in its own plane with a constant velocity (normal to the jet). Apart from the possible practical interest of these cases, the solutions herein derived are mainly offered as additional simple instances of similar three-dimensional laminar flow fields.

According to the remarks made in Ref. 3, similar solutions for the subject flow fields, if existing at all, must be particular solutions of the ordinary differential equations found in Refs. 4 and 5. Therefore, rather than duplicating the usual procedure connected with the "search for similar solutions" we start directly from these ordinary differential equations.

If (x, y, z) is a cartesian reference frame, z the coordinate normal to the body and (u, v, w) the corresponding velocity components, a particular class of three-dimensional similar flow fields is defined by[4,5]:

$$u = Ux^n F'(\eta) \qquad v = Vx^m G'(\eta)$$

$$w = -\frac{U^{1/2}}{K} x^{(n-1)/2}\left[\frac{n+1}{2} F(\eta) + \frac{n-1}{2}\eta F'(\eta)\right]$$

$$\eta = Kz(Ux^{n-1})^{1/2} \quad (1)$$

where U, V, K, n and m are arbitrary constants, η is the similarity variable, primes denote differentiation with respect to η, and the functions F and G satisfy the equations[4,5]:

$$F''' + FF'' - [2n/(n+1)]F'^2 = 0 \quad (2)$$

$$G''' + FG'' - [2m/(n+1)]F'G' = 0 \quad (3)$$

where we have already taken into account that for a wall-jet problem the velocity must vanish[2] far away from the wall (i.e., $F'(\infty) = G'(\infty) = 0$). Since the "independence principle" holds, we can consider Eqs. (2) and (3) separately. We will say that a similar solution for the aforementioned flow fields is "found" if the pertinent physical boundary conditions, when formulated in terms of the functions F and G, are consistent with Eqs. (1) and lead to a solution of Eqs. (2) and (3). In both cases treated herein, the wall is impermeable: hence $u(0) = w(0) = 0$ and, from Eqs. (1), $F(0) = F'(0) = 0$ so that the boundary conditions for Eq. (2) are homogeneous. Glauert[2] has shown that a nontrivial solution without reverse-flow exists only for $n = (-\frac{1}{2})$ and is given by

$$F = h^2 \qquad F' = \tfrac{2}{3}h(1-h^3)$$

$$\eta = \ln\left[\frac{(1+h+h^2)^{1/2}}{1-h}\right] + (3)^{1/2}\, tn^{-1}\left[\frac{h(3)^{1/2}}{2+h}\right] \quad (4)$$

Substitution of these relations into Eq. (3) yields, with $G'(\eta) = H(h)$

$$(d^2H/dh^2) - [24mh/(1-h^3)]H = 0 \quad (5)$$

Consider first the case of a plane jet impinging diagonally on an infinite plane (x being the distance from the axis of the jet). Then $v(0) = v(\infty) = 0$ or, from Eqs. (1) $G'(0) = G'(\infty) = 0$, so that the boundary conditions for Eq. (5) are $H(0) = H(1) = 0$. Nontrivial solutions can be obtained only for well-defined values (eigenvalues) of m. It can be shown that the first few eigenvalues are

$$m_1 = -\tfrac{1}{2} \qquad m_2 = -\tfrac{7}{4} \qquad m_3 = -\tfrac{15}{4}$$

The solution for the first eigenvalue ($m_1 = -\frac{1}{2}$) is rather obviously $H = Ch(1-h^3)$ where C is an arbitrary constant; i.e., G' proportional to F'. Thus the cross-velocity profile is proportional to the main velocity profile. It can be easily argued that the proportionality factor must be equal to the corresponding proportionality factor between the jet velocity components normal and tangential to the wall. The solutions corresponding to the other eigenvalues exhibit a "reverse-flow" behavior. Thus, for instance, the solution for $m = -\frac{7}{4}$ is given by

$$G_1'(\eta) = H(h) = h(1-h^3)(1-\tfrac{5}{2}h^3) \quad (6)$$

as it can be easily checked by direct substitution. This solution is plotted in Fig. 1 together with the solution $G' = h(1-h^3)$ (Glauert profile). At this stage there does not seem to be any support for the actual physical occurrence of these reverse cross-flows, so that, until further evidence, solutions such as that given by Eq. (6) have only a mathematical sig-

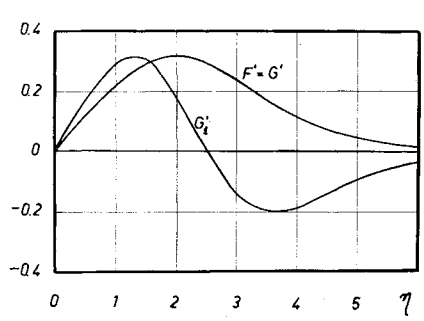

Fig. 1 Cross-velocity profiles for nonorthgonal plane-wall jet corresponding to the first and second eigenvalue.

Received April 26, 1965. This work has been sponsored by the Comitato Nazionale delle Ricerche.

* Director, Institute of Aerodynamics. Member AIAA.

† Research Assistant, Institute of Aerodynamics.